

On the happiness of ferroelectric surfaces and its role in water dissociation: the example of bismuth ferrite

Ipek Efe,¹ Nicola A. Spaldin,¹ and Chiara Gattinoni^{1, a)}

Materials Theory, Department of Materials, ETH Zürich, Wolfgang-Pauli-Strasse 27, 8093, Zürich, Switzerland

(Dated: 18 March 2024)

We investigate, using density functional theory, how the interaction between the ferroelectric polarization and the chemical structure of the (001) surfaces of bismuth ferrite influences the surface properties and reactivity of this material. A precise understanding of the surface behavior of ferroelectrics is necessary for their use in surface science applications such as catalysis as well as for their incorporation in microelectronic devices. Using the (001) surface of bismuth ferrite as a model system we show that the most energetically favoured surface geometries are combinations of surface termination and polarization direction that lead to uncharged, stable surfaces. On the unfavorable charged surfaces, we explore the compensation mechanisms of surface charges provided by the introduction of point defects and adsorbates, such as water. Finally, we propose that the special surface properties of bismuth ferrite (001) could be used to produce an effective water splitting cycle through cyclic polarization switching.

^{a)}Electronic mail: chiara.gattinoni@mat.ethz.ch

The following article has been submitted to the Journal of Chemical Physics.

I. INTRODUCTION

Transition metal oxides occupy a prominent place in heterogeneous catalysis, and are nowadays the most used industrial catalyst type¹. A variety of industrially relevant processes, for example water splitting or the degradation of pollutant molecules, however, still lack an efficient catalyst. In the search of novel catalytic materials, the Sabatier principle, which states that effective catalysis occurs when the adsorption between a molecule and a surface is of intermediate strength, is a limiting factor². However, the adsorption strength between a molecule and the surface can be controlled by utilizing oxides with tunable functionalities, such as piezo- and ferroelectricity³, and research in this field is flourishing⁴⁻⁷. In particular, there is great potential for the use of ferroelectric thin films⁸ or nanoparticles^{5,6,9} in electricity generation, water remediation or drug delivery^{4,7}.

Ferroelectric materials present a spontaneous switchable bulk polarization, and their surfaces, where reactions occur, are complex. In particular, the ferroelectric polarization results in surface bound charges which need to be compensated in order to avoid a polar discontinuity¹⁰. Thus, the surface structure of a ferroelectric and, as a consequence, its reactivity are largely determined by the interplay between bound charges and compensation mechanisms^{11,12}.

Much progress has been made in our understanding of ferroelectricity at a material's surface. Indeed, it is now well understood that compensation of the ferroelectric bound charges at a surface occurs preferentially through adsorbates and defect formation rather than by electronic reconstructions¹²⁻¹⁵. It has also been shown that switching of the surface polarity can be used to promote catalysis for molecular dissociation³. The precise structure of the surface has also been shown to influence the strength and direction of the ferroelectric polarization in thin films, and engineering of surface stoichiometry has been used to manipulate the polarization on ferroelectric surfaces^{11,16-20}.

There are still, however, many open questions regarding the surface science of ferroelectrics⁸. In particular, how the ionic charge in the layers of ferroelectric perovskites interact with the ferroelectric polarization, and the effect of this interplay on the surface structure, is still poorly understood. Here, we investigate this question in bismuth ferrite (BFO), a material which has a robust

ferroelectric polarization at room temperature and, in the (001) direction, neighboring positively-charged $\text{Bi}^{3+}\text{O}^{2-}$ and negatively-charged $\text{Fe}^{3+}\text{O}_2^{2-}$ layers (see Fig. 1a). It is also an especially promising catalyst for applications in water remediation⁹, water splitting^{6,21} and nanoscale drug delivery⁵. In the following, we investigate the stability of the (001) surface of BFO, including the interaction of the polarization with defects and water molecule adsorbates. Our findings allow us to propose a catalytic cycle for efficient water splitting taking advantage of the special properties of BFO (001) surfaces.

II. METHODS

Density functional theory calculations were performed within the periodic supercell approach using the VASP code²²⁻²⁵. The optB86b-vdW functional²⁶, a revised version of the van der Waals (vdW) density functional of Dion *et al.*²⁷, was used throughout, as it has been shown to describe well molecular adsorption on transition metal oxides²⁸⁻³⁰. Core electrons were replaced by projector augmented wave (PAW) potentials³¹, while the valence states ($5e^-$ for Bi, $8e^-$ for Fe and $6e^-$ for O) were expanded in plane waves with a cut-off energy of 500 eV. In all calculations we used slabs with a $\sqrt{2}a \times \sqrt{2}a$ surface area and $4a$ height (shown in Fig. 1a), where a is the lattice parameter of the pseudocubic unit cell. Using the optB86b-vdW functional the pseudocubic lattice parameter was calculated to be $a = 3.95 \text{ \AA}$, with the γ angle in the rhombohedral structure being $\gamma = 90.23^\circ$. The difference of the calculated lattice parameters with respect to the experimental structure is below 0.5%³². A Monkhorst-Pack k -point grid of $(5 \times 5 \times 1)$ was used for all calculations. An antiferromagnetic G-type ordering was imposed, which gave a magnetic moment of $4.2 \mu_B$ per Fe ion in the bulk. The BFO (001) slabs had a thickness of four cubic unit cells and were separated from their periodic repetitions in the direction perpendicular to the surface by $\sim 20 \text{ \AA}$ of vacuum. Upon testing we found that this thickness was sufficient to converge the adsorption energies of the water molecules (see Table S1). A dipole correction along the direction perpendicular to the surface was applied, and geometry optimizations were performed with a residual force threshold of 0.01 eV/\AA . BFO has a large intrinsic polarization, \mathbf{P} , whose experimental value is $\sim 0.9 \text{ C/m}^2$ along the (111) direction³³; we calculated \mathbf{P} with the formula:

$$\mathbf{P} = \frac{e}{V} \sum_{m=1}^N Q_m \mathbf{u}_m, \tag{1}$$

where e is the charge of the electron, V the unit cell volume, N the number of atoms in the unit cell and \mathbf{u} the atomic displacements from the high symmetry positions. We obtained a value of $P=0.86 \text{ C/m}^2$ when using the formal charges for Q and of $P=1.19 \text{ C/m}^2$ when using the Born effective charges.

Adsorption energies for the water molecules, E_{ads} , were calculated as:

$$E_{\text{ads}} = (E_{\text{water/BFO}} - E_{\text{BFO}} - n \times E_{\text{water}}) / n, \quad (2)$$

where E_{BFO} , E_{water} and $E_{\text{water/BFO}}$ are the total energies of the relaxed bare slab, an isolated gas phase water molecule and a system containing n water molecules adsorbed on the slab, respectively. Negative values of the adsorption energy indicate favorable (exothermic) adsorption. Water coverages varying between 1/2 and 1 monolayer (ML) — where 1 monolayer is one water molecule per surface metal atom — were considered.

To calculate the charge density differences of Fig. 4 we first obtained the real-space charge for the slab/water system (ρ_{all}) and for the isolated slab (ρ_{slab}) and water molecules (ρ_{water}). The difference was then obtained as:

$$\rho_{\text{diff}} = \rho_{\text{all}} - \rho_{\text{slab}} - \rho_{\text{water}}. \quad (3)$$

III. RESULTS AND DISCUSSION

BFO (001) has interesting surface properties when we consider the interplay between layer charge and ferroelectric polarization, and they are schematically shown in Fig. 1. The formal charges of Bi^{3+} , Fe^{3+} and O^{2-} result, in the (001) direction, in alternating positively charged BiO ($+1 \text{ C/m}^2$) and negatively charged FeO_2 (-1 C/m^2) layers, see Fig. 1a. This surface charge requires a compensating charge of opposite sign and half the magnitude^{10,34} ($\sim \pm 0.5 \text{ C/m}^2$, negative for BiO and positive for FeO_2) to obtain surface stability. Remarkably (and coincidentally), the (001) component of the ferroelectric polarization in BiFeO_3 has the value $P \sim \pm 0.5 \text{ C/m}^2$ (resulting in the surface charge density of $\sim \pm 0.5 \text{ C/m}^2$), positive when the polarization is directed towards the surface and negative when away from the surface. Thus, the interplay of these two contributions of equal magnitude can result either in fully self-compensating surfaces with a total surface charge density $\sigma = 0 \text{ C/m}^2$ in which the surface polarization compensates the layer charge, or highly uncompensated surfaces in which both the layer charge and the surface polarization are contribute to a non-zero surface charge.³⁵ The self-compensating case, shown in Fig. 1b, occurs

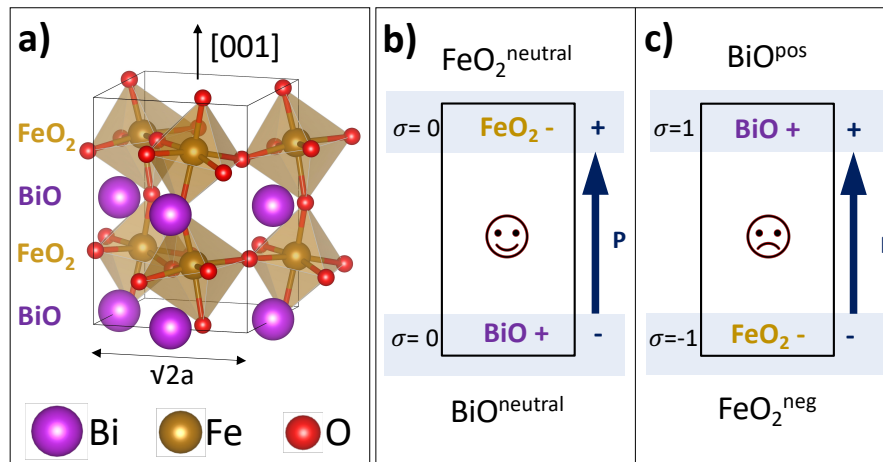


FIG. 1. (a) Unit cell of bismuth ferrite used in this work, with the axes oriented along the (001) and, in plane, the (110) and $(\bar{1}\bar{1}0)$ crystallographic directions. The formal charges of the atoms are Bi^{+3} , Fe^{+3} , O^{-2} . Purple represents Bi, gold Fe and red O atoms. (b) The favorable polarization direction which creates charge-compensated surfaces points from the BiO to the FeO_2 termination. (c) The unfavorable polarization direction which creates polar surfaces points from the FeO_2 towards the BiO surface termination. σ is the surface charge density in C/m^2 units.

in BiO surfaces with the polarization pointing away from them (we will refer to these surfaces as $\text{BiO}^{\text{neutral}}$) and FeO_2 surfaces with the polarization pointing towards them ($\text{FeO}_2^{\text{neutral}}$). The highly uncompensated surfaces, shown in Fig. 1c, are, instead, the BiO (FeO_2) surfaces with the polarization pointing towards (away from) them and we will refer to these surfaces as BiO^{pos} and $\text{FeO}_2^{\text{neg}}$.

In this work we study the two stoichiometric (001) systems shown in Fig. 1b and c. In panel b there is a fully compensated BFO (001) slab which we will refer to as the “happy” system, since the full surface charge compensation means that there is no polar discontinuity at the surface and the polarization is stable. The uncompensated slab of panel c will be referred to as the “unhappy” system, because the non-zero surface charge density results in an unphysical polar discontinuity, and the surface charge needs to be compensated to render the surface stable¹⁰.

In the following we explore ways to stabilize the polarization in the unhappy system both with defect engineering and molecular adsorption. In particular, we investigate how the different surface electronic properties of the two slabs—their “happiness”, if you will—affect the geometry and adsorption strength of water. We show that the resulting polarization-dependent dissociation behavior has great potential for catalytic applications.

A. Achieving surface stability through point defect engineering

It is known that point defects and adsorbates can provide charge compensation to ferroelectric surfaces^{3,11,12}. As already remarked, the self-compensating surfaces of the happy system have no polar discontinuity and do not require any further compensation. Indeed, our calculated unit cell by unit cell polarization plotted in Fig. 2a shows that the ferroelectric polarization is stable throughout the slab thickness. Upon geometry relaxation, the unhappy slab also relaxes into the structure of Fig. 2a, meaning that in order to avoid the polar discontinuity at the surface, the polarization direction reverses, resulting in a happy system. This indicates that the polarization direction in the unhappy system cannot exist without a means to compensate the surface charges.

To stabilize the unhappy system we consider Bi and O adatoms and vacancies: the positively charged Bi adatom and O vacancy compensate the negatively charged $\text{FeO}_2^{\text{neg}}$ surface, the negatively charged Bi vacancy and O adatom compensate the positive BiO^{pos} surface. Bi defects, rather than Fe ones, are considered here as they are seen to occur more often in experiments³⁶.

Fig. 2b shows the geometry-optimized structure and the unit cell by unit cell polarization in the unhappy slabs compensated with point defects at both surfaces. We note that, indeed, compensation of the surface charges by vacancies and adatoms is effective in stabilizing the downward-pointing polarization direction in the unhappy slab. We also observe surface enhancements of the polarization above the bulk value of $90 \mu\text{C}/\text{cm}^2$, especially at the surfaces where O and Bi adatoms are present, which are driven by the surface chemistry. In particular the bonding between a surface Bi and the O adatom (top of Fig. 2b) pulls the Bi atom away from the surface, enhancing the polarization at the BiO surface of the slab.

We also investigated partial compensation of the slab, by including point defects on only one surface, rather than both. This allows us to understand whether compensation from one surface only is sufficient to ensure stable polarization throughout the slab thickness, and also to separately investigate the BiO^{pos} and $\text{FeO}_2^{\text{neg}}$ surfaces. The results are shown in Fig. 2c.

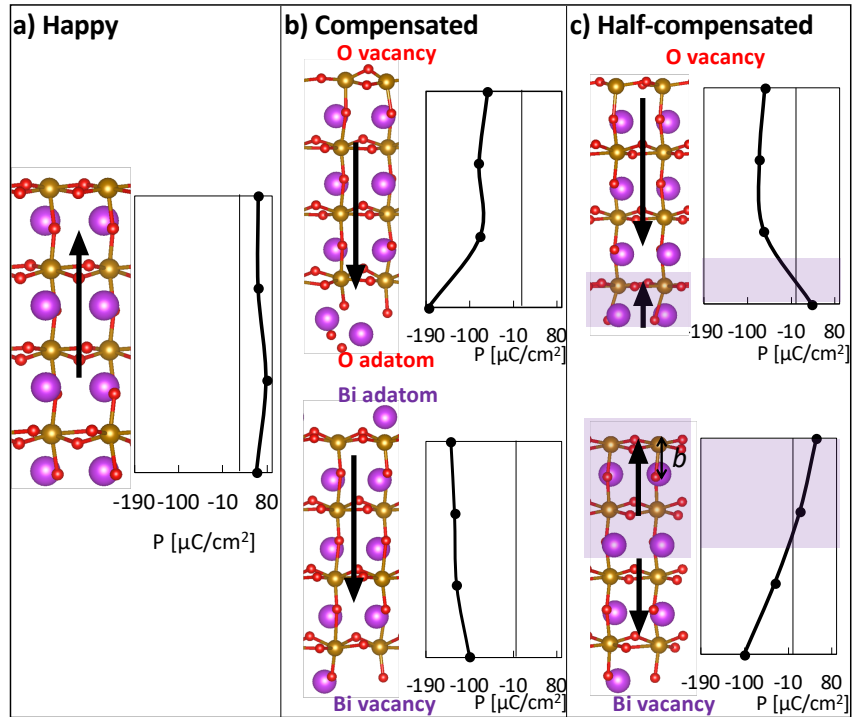


FIG. 2. Calculated structures and corresponding layer-by-layer polarization for a range of a four unit cell-thick BFO (001) slabs. a) Happy system. P is constant throughout the slab thickness without further compensation. b) Unhappy slabs with surface charges compensated by O (top) and Bi (bottom) defects. c) unhappy slab with partial compensation of the surface charges. Compensation of the FeO_2 surface with an oxygen vacancy (top) and of the BiO surface with a Bi vacancy (bottom). The bond between surface Ti and subsurface O atoms is shown as b . The purple shading indicates areas of polarization reversal. The black arrows indicate the polarization direction.

On the non-compensated side of the slab polarization reversal occurs, confirming that compensation on both surfaces is needed to obtain a robust polarization throughout the thickness. In the uncompensated BiO^{pos} termination (top of Fig. 2c), polarization reversal occurs only in the outermost BiO surface layer (shown in purple shading), the polarization pointing away from the BiO surface. For an uncompensated $\text{FeO}_2^{\text{neg}}$ surface (bottom of Fig. 2c) the polarization reversal (purple shading) involves the topmost two unit cells and the polarization points towards the surface. Thus, both uncompensated surfaces become happy by this reversal of the polarization. The problem of charge compensation now occurs within the slab, where the positive (in the top of Fig. 2c) and the negative (in the bottom of Fig. 2c) ends of the polarization meet creating a polar discontinuity.

Charge compensation in the bulk forces a metallic layer at the site of the polar discontinuity, which requires band bending. The energy cost of the band bending is however offset by the favorable — happy — surface configuration. However, also the local surface chemistry drives this surface structure. On BiO^{pos} the cation has a lone pair of electrons which orients towards the vacuum, pushing the ion towards the subsurface (here, FeO_2) layer and creating a ferroelectric polarization pointing away from the surface, and, as a consequence a $\text{BiO}^{\text{neutral}}$ surface. A similar behavior is observed for the PbO surface of lead titanate¹¹ which also has a lone pair of electrons. On $\text{FeO}_2^{\text{neg}}$ the bond labelled b in Fig. 2c is shorter than in the bulk, as it is generally the case for atomic bonds between the two topmost layers of a slab³⁷. This shorter bond b forces the Bi lone pair downwards and the ion upwards, thus imposing a polarization which points towards the surface, which persists, to a lesser degree, in the unit cell below. Note that in the previous example of lead titanate, no polarization inversion is observed for the TiO_2 termination with the polarization pointing away from it¹¹. The difference in behavior between these two ferroelectric perovskites is probably due to the higher relative polarizability of Ti^{4+} compared to Fe^{3+} .

Having shown how intrinsic point defects can stabilize the ferroelectric polarization in the unhappy systems, we now investigate how stability can be obtained through adsorbates, by examining the behavior of water on BFO (001).

B. Achieving stability through adsorbates: the example of water

As well as intrinsic surface defects, adsorbates can play an important role in shaping the surface structure of a ferroelectric¹². The interaction of a surface with water is especially important because of water’s ubiquity in air and in solutions, and also because of the potential for applications which arise from the interaction between water and functional materials. In the following, we analyse the behavior of water adsorbed on the surfaces of the systems in Fig. 1b and c, and reveal how water can stabilize the unhappy system and, in turn, how surface charges affects the water adsorption energy and propensity for dissociation.

1. Water adsorption on a happy surface

We identified the most stable sites for water adsorption on the surfaces of the happy system, and they are shown in Fig. 3. On $\text{FeO}_2^{\text{neutral}}$, the most favorable configuration for molecular H_2O

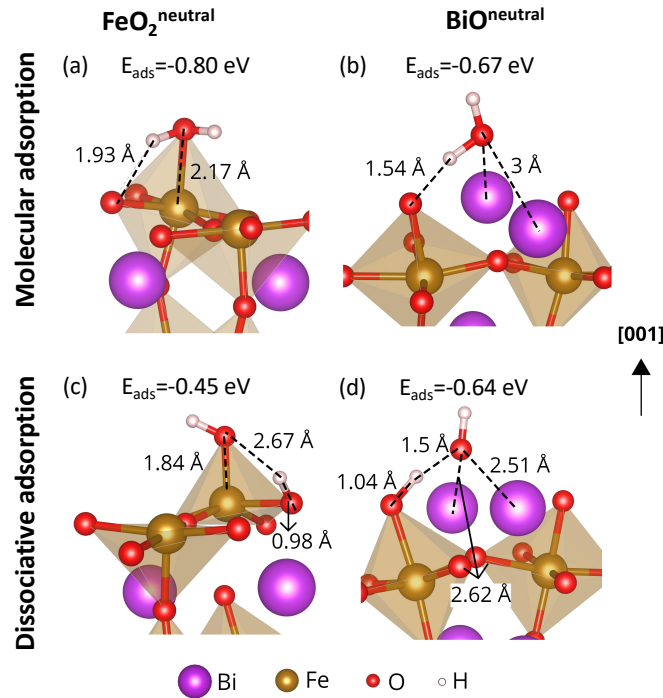


FIG. 3. The most favorable adsorption sites for the adsorption of a water molecule, their adsorption energies and the bond distances between the water molecule and the surface ions for the two happy terminations. Molecular adsorption of a water molecule on the (a) $\text{FeO}_2^{\text{neutral}}$ and (b) $\text{BiO}^{\text{neutral}}$ termination. Dissociative adsorption of a water molecule on (c) $\text{FeO}_2^{\text{neutral}}$ and (d) $\text{BiO}^{\text{neutral}}$ termination. Purple indicates Bi, gold Fe, red O and white H atoms.

adsorption is parallel to the surface with the formation of a 2.17 Å Fe-O bond and of a 1.93 Å H- O_{surf} (O_{surf} is a surface oxygen) bond (see Fig. 3a). For the $\text{BiO}^{\text{neutral}}$ termination, the water O atom sits at the bridging site between two Bi atoms, aligned perpendicularly to the surface. This configuration permits only one hydrogen bond of length 1.54 Å (Fig. 3b). Indeed, charge density difference calculations, presented in Fig. 4b, show that minimal charge transfer between the water O and the Bi surface atom occurs. The water-surface binding is stronger on the $\text{FeO}_2^{\text{neutral}}$ termination than on the $\text{BiO}^{\text{neutral}}$ by ~ 0.13 eV, since in the former molecular adsorption is established by a strong ionic bond and a hydrogen bond (Fig. 4a).

For a dissociated water molecule, the favored binding sites for the hydroxyl groups are a surface Fe for the $\text{FeO}_2^{\text{neutral}}$ termination (see Fig. 3c) and the Bi-Bi bridging site for the $\text{BiO}^{\text{neutral}}$ termination (see Fig. 3d), similar configurations to the molecularly adsorbed water. Also, the rotation of the hydroxyl with respect to the surface is similar to that of the intact water molecule:

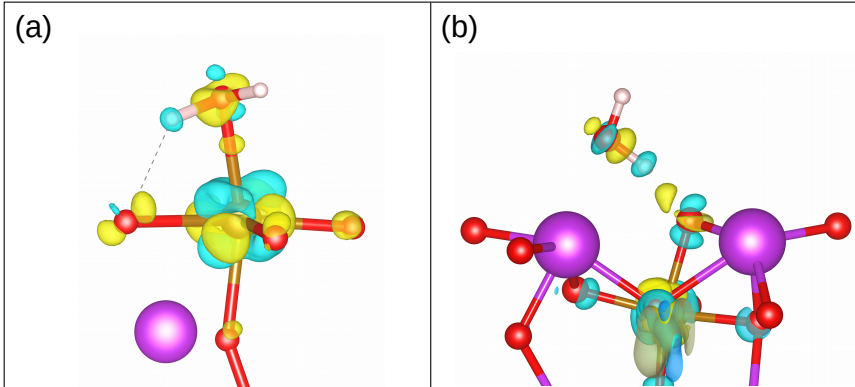


FIG. 4. Charge density differences ρ_{diff} , calculated using Eq. 3, for molecular H_2O adsorption on the (a) FeO_2 and (b) BiO termination. Light blue represents electron density reduction while yellow represents the electron density increase. The isosurface level is 0.01 e/volume.

parallel to the surface on $\text{FeO}_2^{\text{neutral}}$ and perpendicular on $\text{BiO}^{\text{neutral}}$. In both cases the H ion binds to an O_{surf} (Fig. 3c-d).

The adsorption energies in Fig. 3 and Table I show that dissociation of the water molecule is disfavoured on both compensated terminations of a happy BFO (001) slab, by ~ 30 meV for $\text{BiO}^{\text{neutral}}$ and ~ 350 meV for $\text{FeO}_2^{\text{neutral}}$.

It is worth noting that in all systems the polarization throughout the film is bulk-like and minimally affected by the adsorption of either molecular or dissociated H_2O .

2. Water adsorption on an unhappy surface

We next turn our attention to the adsorption of water on the unhappy slab with $\text{FeO}_2^{\text{neg}}$ and BiO^{pos} surfaces, and we find that on this system dissociative water adsorption is favored.

Since the unhappy slab is unstable, calculations of the BFO/water system in this section are performed with a “frozen” BFO slab: we kept the ionic positions of the inner layers of the slab fixed at the bulk values and allowed only the adsorbed molecules and topmost surface layer, where adsorption occurs, to relax. The “frozen” layers are shown in blue shading in Fig. 5a. We refer to the adsorption energies with respect to this “frozen” substrate as $E_{\text{ads}}^{\text{frozen}}$.

We simulated molecularly and dissociatively adsorbed water on the $\text{FeO}_2^{\text{neg}}$ and BiO^{pos} surfaces, and we observed similar adsorption geometries as on the happy slab, both in the preferred

adsorption sites and bond lengths (the structures are shown in Fig. S1). Indeed, on $\text{FeO}_2^{\text{neg}}$ the water molecule and the hydroxyl adsorb parallel to the surface; on BiO^{pos} they adsorb perpendicularly to the surface in the Bi-Bi bridge site. However, the energy trends are significantly different from the happy case, and dissociative adsorption is favorable on these uncompensated surface terminations. Indeed, the values in Table I show that dissociative adsorption is favored by 290 meV on the $\text{FeO}_2^{\text{neg}}$ surface and by 160 meV on BiO^{pos} .

It is worth noting that, despite the similarities in the adsorption geometries, there are significant differences between the electronic structures of the happy and unhappy systems, as highlighted in the local density of state (*IDOS*) of the surface layers and adsorbates in Fig. 5a. In the happy system (left), the *IDOS* of both $\text{FeO}_2^{\text{neutral}}$ and $\text{BiO}^{\text{neutral}}$ surface layers presents an insulating behavior with a ~ 2 eV-wide band gap around the Fermi level, as in bulk BFO. The conduction and valence band edges on both $\text{FeO}_2^{\text{neutral}}$ and $\text{BiO}^{\text{neutral}}$ are at the same energy, showing that the ferroelectric polarization is well screened and no band bending occurs through the slab. Conversely, the $\text{FeO}_2^{\text{neg}}$ and BiO^{pos} surfaces in the unhappy system (right of Fig. 5a) are metallic, since the large surface charge of $\pm 1 \text{ C/m}^2$ is compensated by electrons (BiO^{pos}) and holes ($\text{FeO}_2^{\text{neg}}$)¹⁰.

When water is molecularly adsorbed on happy and unhappy surfaces alike (dashed lines in the graphs in Fig. 5a), the *IDOS* of the water molecules and of the surface overlap away from the Fermi level and the position of the band edges have only a small effect on the water/surface interaction. This can explain the similar adsorption energies for intact water on the happy and unhappy system, see Table I. The increased stability in the adsorption energy of dissociated water on the unhappy system can instead be related to a partial compensation of the surface charge by the OH^- (on BiO^{pos}) and H^+ (on $\text{FeO}_2^{\text{neg}}$), which results in change in the *IDOS* at the Fermi level for the unhappy surfaces (especially on $\text{FeO}_2^{\text{neg}}$).

System	FeO ₂		BiO		Adsorption on both sides	
	Intact	Dissociated	Intact	Dissociated	Intact	Dissociated
Happy	-0.80	-0.45	-0.67	-0.64	-0.75	-0.60
Unhappy (frozen slab)	-0.90	-1.19	-0.57	-0.73	-0.60	-0.92
Stabilized (frozen slab)	—	—	—	—	—	-3.16
Stabilized (relaxed slab)	—	—	—	—	—	-0.47

TABLE I. Adsorption energies for 0.5 ML of water adsorbed on the BiO and FeO₂ surfaces of BFO (001)

The molecular adsorption of water on an unhappy slab does not provide adequate charge transfer to stabilize the unfavorable polarization direction, and neither does the co-adsorption of hydroxyl and H on the same surface. Indeed, for these structures, when we allow the ions in the “frozen” slab to relax into their energetically favorable position, we obtain a happy system. However, stabilization of the polarization in the unhappy system can be achieved when 1 ML of OH^- is adsorbed on the positively charged BiO^{pos} termination and 1 ML of H^+ on the negatively charged $\text{FeO}_2^{\text{neg}}$ termination, thus fully compensating the surface charges of $\pm 1 \text{ C/m}^2$. The adsorption structure is, as expected, at a Bi-Bi bridge site for the hydroxyl groups and atop an O_{surf} atom for the H atoms. We will refer to this configuration as the “stabilized system” and it is shown in Fig. 5b.

The stabilized system is the most stable among the computed water structures on unhappy BFO. Indeed, the adsorption energy of dissociated water in the stabilized system, with respect to the frozen substrate is $E_{\text{ads}}^{\text{frozen}} = -3.16 \text{ eV/mol}$, much larger than the values (reported in Table I) for the structures examined in Fig. 5a.

Since the unhappy ferroelectric polarization (from FeO_2 to BiO) in the stabilized system in Fig. 5b is now fully compensated, we can relax the ionic positions of the whole slab. We obtain an adsorption energy for the fully relaxed stabilized system (with respect to relaxed happy slab) of $E_{\text{ads}} = -0.47 \text{ eV/mol}$. In comparison, water adsorbed on the happy system leads to a more negative (by 0.2 eV/mol) adsorption energy, see Table I, and thus to a more energetically favorable structure. This comparison tells us that the system in Fig. 5b, despite being stable, will not occur spontaneously, but will be reached by switching the polarization with an external electric field.

C. Discussion

The results presented in this work show the complex coupling between the surface chemistry and the ferroelectric polarization at the (001) surfaces of BFO. The $\text{BiO}^{\text{neutral}}$ and $\text{FeO}_2^{\text{neutral}}$ terminations of BFO (001) surfaces are charge neutral, thanks to the interaction between layer charge and ferroelectric bound charges. Upon reversal of the polarization, both surface terminations BiO^{pos} and $\text{FeO}_2^{\text{neg}}$ present a large surface charge that can be effectively compensated by point defects or by dissociated water molecules. Upon growth of ferroelectric films and nanocrystals, it is very difficult to obtain defect-free surfaces, and these results point to which defects are likely to occur. Moreover, the surface defect engineering could be important during thin-film growth of

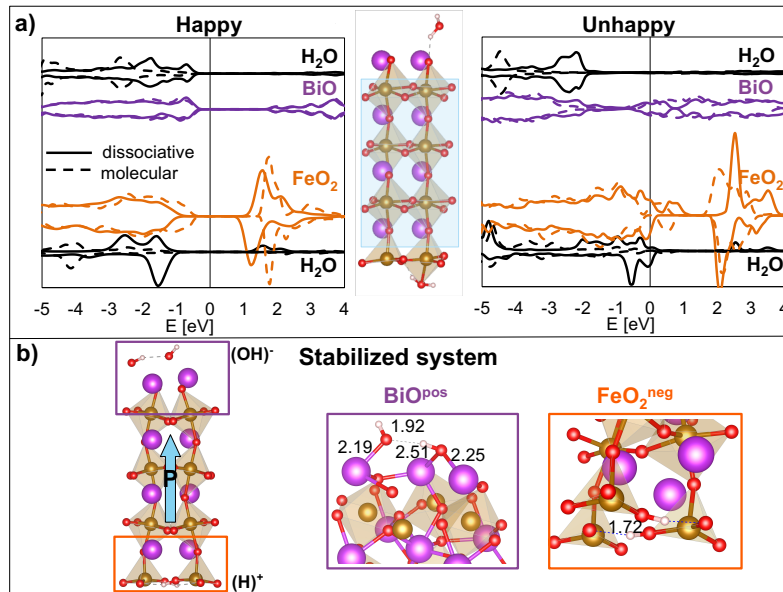


FIG. 5. (a) Local density of state (*LDOS*) for the surface layers and water molecules for the "happy" (top) and "unhappy" (bottom) systems. The *LDOS* for water is in black, for the BiO layer in purple and for the FeO₂ layer in orange. The black vertical line at E=0 eV is the Fermi level. The dashed (solid) lines are the *LDOS* for molecularly (dissociatively) adsorbed water. A representative system is shown in the middle. The light blue shading indicates the BFO layers which are kept frozen in the calculations of the unhappy system. (b) Stabilized system with two water molecules adsorbed dissociatively with OH groups on the BiO termination and H atoms on the FeO₂ termination.

unhappy ferroelectric surfaces, where defect formation could be engineered to stabilize or even enhance the surface polarization^{11,38}.

Now we focus on water adsorption and dissociation. Our calculations reveal that the adsorption mode of water on stoichiometric BFO (001) is highly dependent on the combination of polarization direction and surface termination. Indeed, we find that compensated surfaces favor the molecular adsorption of water, uncompensated ones dissociative adsorption. The obtained adsorption structures are in good agreement with previous theoretical work on (001) perovskites, such as strontium ruthenate³⁹, barium hafnate⁴⁰, barium zirconate⁴⁰, strontium titanate⁴¹ and strontium zirconate⁴². All these materials are non ferroelectric and have charge-neutral surfaces, therefore, despite similar adsorption structure, we do not necessarily expect the same behavior and the same energy ordering between the intact and dissociated structures. Indeed, the literature (summarized in Table II in the SI) shows that water can show a range of different adsorption behavior on the sur-

faces of these complex materials. Together with the surface structure, the interplay of many other factors including neutrality of the crystal ionic layers, lattice parameters⁴³ and dielectric/metallic characteristics of the materials should be considered to understand the interface chemistry and structure stability.

We believe that this polarization dependence of water dissociation in bismuth ferrite could have interesting ramifications for catalysis. We propose that the opposite affinity towards water dissociation of the happy and unhappy systems could also be utilized for the creation of a water splitting catalytic cycle, by exploiting the ferro- and piezoelectric properties of BFO as illustrated in Figure 6. The cycle starts with a happy BFO (001) slab which favours molecularly adsorbed water on both $\text{BiO}^{\text{neutral}}$ and $\text{FeO}_2^{\text{neutral}}$ terminations (Figure 6, panel 1). Upon switching of the polarization, we obtain an unhappy slab with charged surfaces. The resulting system favours dissociation of the adsorbed water molecules on BiO^{pos} and $\text{FeO}_2^{\text{neg}}$ surfaces (Figure 6, panel 2). Our calculations then indicate that selective desorption of the H^+ ion from the BiO^{pos} termination and OH^- group from the $\text{FeO}_2^{\text{neg}}$ termination is favorable as it stabilizes the polarization by compensating the surface charges (Figure 6, panel 3). By further switching of the polarization back into its initial happy direction, competitive adsorption would favor the further removal of dissociation products and the adsorption of molecular H_2O (Figure 6, panel 4). Thus, in principle, cyclical switching of the polarization in a BFO (001) slab immersed in water could efficiently produce H and OH species, which can then be used directly in, *e.g.* the degradation of pollutants⁹, or for H_2 production together with a metal cathode. Polarization switching in nanoscale BFO can be obtained not only with an electric field, but also through mechanical strain⁴⁴. It could thus be economically achieved with, for example, sound waves⁹. We hope that this thought experiment can pave the way for the creation of an effective BFO-based water splitting device.

ACKNOWLEDGMENTS

C. G. is supported by the European Union’s Horizon 2020 research and innovation programme under the Marie Skłodowska-Curie grant agreement No. 744027. N.A.S. acknowledges funding from the European Research Council (ERC) under the European Union’s Horizon 2020 research and innovation programme grant agreement No 810451. I. E. acknowledges the use of the Euler cluster managed by the HPC team at ETH Zurich. C. G.’s work was supported by a grant from the Swiss National Supercomputing Centre (CSCS) under project ID s889.

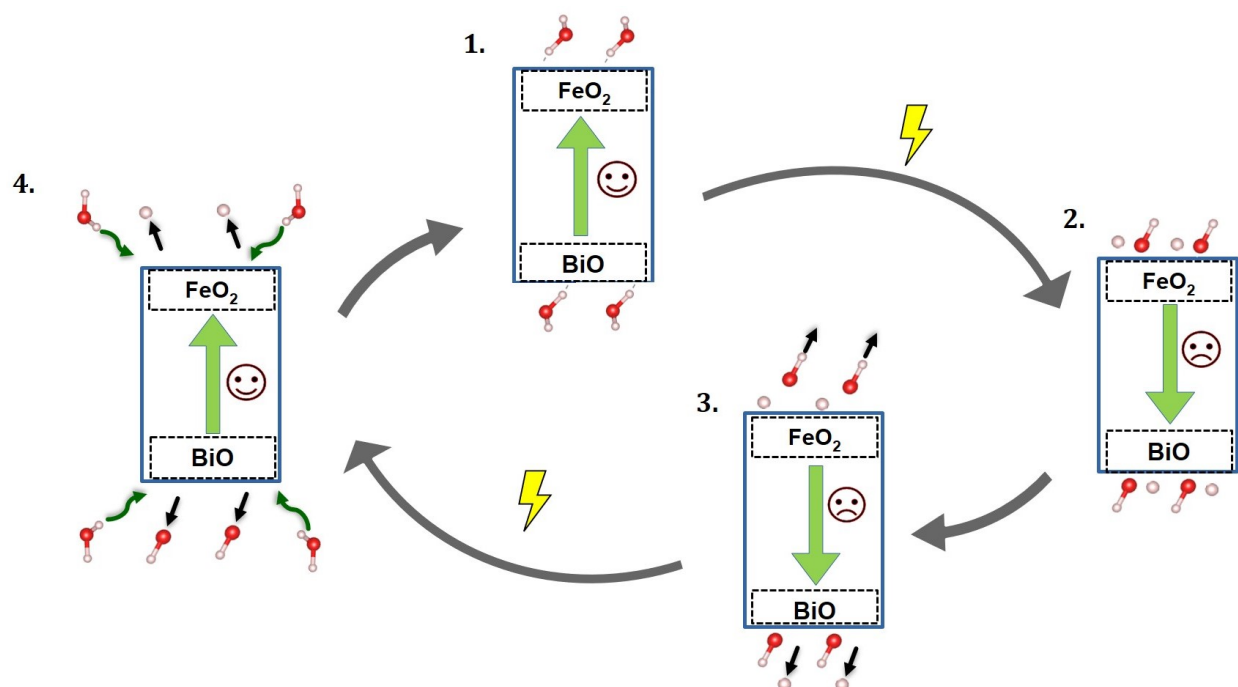


FIG. 6. Demonstration of the proposed cyclic process for a water splitting device. (1) Water is adsorbed molecularly on both terminations when the slab is spontaneously polarized in the favorable polarization direction. (2) Switching of the polarization via an external electric field forces the molecularly adsorbed molecules to dissociate on the surface. (3) Selective desorption of the functional groups carrying the same-sign charge with the surfaces. Different functional groups of the water molecules are separated on the opposite surfaces. (4) Desorption of the dissociatively adsorbed groups after switching the polarization back to the favorable direction followed by molecular adsorption of a water molecule.

DATA AVAILABILITY

The data that supports the findings of this study are available within the article and its supplementary material.

REFERENCES

- ¹J. V'edrine, "Heterogeneous catalysis on metal oxides," *Catalysts* **7**, 341 (2017).
- ²A. Vojvodic and J. K. Nørskov, "New design paradigm for heterogeneous catalysts," *Nati. Sci. Rev.* **2**, 140–143 (2015).

- ³A. Kakekhani and S. Ismail-Beigi, “Ferroelectric oxide surface chemistry: water splitting via pyroelectricity,” *J. Mater. Chem. A* **4**, 5235–5246 (2016).
- ⁴N. A. Spaldin, “Multiferroics beyond electric-field control of magnetism,” *Proc. Royal Soc. A* **476**, 20190542 (2020).
- ⁵M. Salim, D. Salim, D. Chandran, H. S. Aljibori, and A. S. Kherbeet, “Review of nano piezoelectric devices in biomedicine applications,” *J. Intelligent Mat. Sys. Str.* **29**, 2105–2121 (2018).
- ⁶M. B. Starr and X. Wang, “Fundamental analysis of piezocatalysis process on the surfaces of strained piezoelectric materials,” *Sci. Rep.* **3**, 2160 (2013).
- ⁷C. R. Bowen, H. A. Kim, P. M. Weaver, and S. Dunn, “Piezoelectric and ferroelectric materials and structures for energy harvesting applications,” *Energy Environ. Sci.* **7**, 25–44 (2013).
- ⁸L. W. Martin and A. M. Rappe, “Thin-film ferroelectric materials and their applications,” *Nature Rev. Mat.* **2**, 16087 (2017).
- ⁹F. Mushtaq, X. Chen, M. Hoop, H. Torlakcik, E. Pellicer, J. Sort, C. Gattinoni, B. J. Nelson, and S. Pané, “Piezoelectrically enhanced photocatalysis with BiFeO₃ nanostructures for efficient water remediation,” *iScience* **4**, 236 (2018).
- ¹⁰M. Stengel, “Electrostatic stability of insulating surfaces: Theory and applications,” *Phys. Rev. B* **84**, 205432 (2011).
- ¹¹C. Gattinoni, N. Strkalj, R. Härdi, M. Fiebig, M. Trassin, and N. A. Spaldin, “Interface and surface stabilization of the polarization in ferroelectric thin films,” *Proc. Nat. Ac. Sc.* **accepted**, — (2020).
- ¹²S. V. Levchenko and A. M. Rappe, “Influence of ferroelectric polarization on the equilibrium stoichiometry of lithium niobate (0001) surfaces,” *Phys. Rev. Lett.* **100**, 256101 (2008).
- ¹³D. D. Fong, A. M. Kolpak, J. A. Eastman, S. K. Streiffer, P. H. Fuoss, G. B. Stephenson, C. Thompson, D. M. Kim, K. J. Choi, C. B. Eom, I. Grinberg, and A. M. Rappe, “Stabilization of monodomain polarization in ultrathin PbTiO₃ films,” *Phys. Rev. Lett.* **96**, 127601 (2006).
- ¹⁴M. Setvin, M. Reticioli, F. Poelzleitner, J. Hulva, M. Schmid, L. A. Boatner, C. Franchini, and U. Diebold, “Polarity compensation mechanisms on the perovskite surface KTaO₃(001),” *Science* **359**, 572–575 (2018).
- ¹⁵K. Garrity, A. Kakekhani, A. Kolpak, and S. Ismail-Beigi, “Ferroelectric surface chemistry: First-principles study of the PbTiO₃ surface,” *Phys. Rev. B* **88**, 045401 (2013).
- ¹⁶R. V. Wang, D. D. Fong, F. Jiang, M. J. Highland, P. H. Fuoss, C. Thompson, A. M. Kolpak, J. A. Eastman, S. K. Streiffer, A. M. Rappe, and G. B. Stephenson, “Reversible chemical switching

- of a ferroelectric film,” *Phys. Rev. Lett.* **102**, 047601 (2009).
- ¹⁷M. J. Highland, T. T. Fister, D. D. Fong, P. H. Fuoss, C. Thompson, J. A. Eastman, S. K. Streiffer, and G. B. Stephenson, “Equilibrium polarization of ultrathin PbTiO_3 with surface compensation controlled by oxygen partial pressure,” *Phys. Rev. Lett.* **107**, 187602 (2011).
- ¹⁸W. A. Saidi, J. M. P. Martirez, and A. M. Rappe, “Strong reciprocal interaction between polarization and surface stoichiometry in oxide ferroelectrics,” *Nano Lett.* **14**, 6711–6717 (2014).
- ¹⁹L. C. Tănase, N. G. Apostol, L. E. Abramiuc, C. A. Tache, L. Hrib, L. Trupină, L. Pintilie, and C. M. Teodorescu, “Ferroelectric triggering of carbon monoxide adsorption on lead zirconate (001) surfaces,” *Sci. Rep.* **6**, 35301 (2016).
- ²⁰Y. Tian, L. Wei, Q. Zhang, H. Huang, Y. Zhang, H. Zhou, F. Ma, L. Gu, S. Meng, L.-Q. Chen, C.-W. Nan, and J. Zhang, “Water printing of ferroelectric polarization,” *Nature Comm.* **9**, 3809 (2018).
- ²¹S. J. A. Moniz, C. S. Blackman, P. Southern, P. M. Weaver, J. Tang, and C. J. Carmalt, “Visible-light driven water splitting over BiFeO_3 photoanodes grown via the lpcvd reaction of $[\text{Bi}(\text{OtBu})_3]$ and $[\text{Fe}(\text{OtBu})_3]_2$ and enhanced with a surface nickel oxygen evolution catalyst,” *Nanoscale* **7**, 16343–16353 (2015).
- ²²G. Kresse and J. Hafner, “*Ab initio* molecular dynamics for liquid metals,” *Phys. Rev. B* **47**, 558 (1993).
- ²³G. Kresse and J. Hafner, “*Ab initio* molecular-dynamics simulation of the liquid-metal–amorphous-semiconductor transition in germanium,” *Phys. Rev. B* **49**, 14251 (1994).
- ²⁴G. Kresse and J. Furthmueller, “Efficiency of ab-initio total energy calculations for metals and semiconductors using a plane-wave basis set,” *Comp. Mat. Sci.* **6**, 15 (1996).
- ²⁵G. Kresse and J. Furthmueller, “Efficient iterative schemes for *ab initio* total-energy calculations using a plane-wave basis set,” *Phys. Rev. B* **54**, 11169 (1996).
- ²⁶J. Klimeš, D. R. Bowler, and A. Michaelides, “Van der Waals density functionals applied to solids,” *Phys. Rev. B* **83**, 195131 (2011).
- ²⁷M. Dion, H. Rydberg, E. Schröder, D. C. Langreth, and B. I. Lundqvist, “Van der Waals density functional for general geometries,” *Phys. Rev. Lett.* **92**, 246401 (2004).
- ²⁸S. Dabaghmanesh, E. C. Neyts, and B. Partoens, “Van der waals density functionals applied to corundum-type sesquioxides: bulk properties and adsorption of CH_3 and C_6H_6 on (0001) surfaces,” *Phys. Chem. Chem. Phys.* **18**, 23139–23146 (2016).

- ²⁹J. Roy, S. Kar, and J. Leszczynski, “Insight into the optoelectronic properties of designed solar cells efficient tetrahydroquinoline dye-sensitizers on $\text{TiO}_2(101)$ surface: first principles approach,” *Sci. Rep.* **8**, 10997 (2018).
- ³⁰A. Lozano, B. Escribano, E. Akhmatkaya, and J. Carrasco, “Assessment of van der Waals inclusive density functional theory methods for layered electroactive materials,” *Phys. Chem. Chem. Phys.* **19**, 10133–10139 (2017).
- ³¹G. Kresse and D. Joubert, “From ultrasoft pseudopotentials to the projector augmented-wave method,” *Phys. Rev. B* **59**, 1758 (1999).
- ³²F. Kubel and H. Schmid, “Structure of a ferroelectric and ferroelastic monodomain crystal of the perovskite BiFeO_3 ,” *Acta Crys. B* **46**, 698–702 (1990).
- ³³T. Rojac, E. Khomyakova, J. Walker, H. Ursic, and A. Bencan, “ BiFeO_3 ceramics and thick films: Processing issues and electromechanical properties,” in *Magnetic, Ferroelectric, and Multiferroic Metal Oxides*, Metal Oxides, edited by B. D. Stojanovic (Elsevier, 2018) pp. 515 – 525.
- ³⁴A. Ohtomo and H. Y. Hwang, “A high-mobility electron gas at the $\text{LaAlO}_3/\text{SrTiO}_3$ heterointerface,” *Nature* **427**, 423–426 (2004).
- ³⁵For a discussion in terms of the Modern Theory of Polarization see Ref. 45.
- ³⁶L. Jin, P. X. Xu, Y. Zeng, L. Lu, J. Barthel, T. Schulthess, R. E. Dunin-Borkowski, H. Wang, and C. L. Jia, “Surface reconstructions and related local properties of a BiFeO_3 thin film,” *Scientific reports* **7**, 39698 (2017).
- ³⁷K. Kern, “Restructuring at surfaces,” in *Surface Science: Principles and Applications*, edited by R. F. Howe, R. N. Lamb, and K. Wandelt (Springer Berlin Heidelberg, Berlin, Heidelberg, 1993) pp. 81–94.
- ³⁸N. Strkalj, C. Gattinoni, A. Vogel, M. Campanini, R. Haerdi, A. Rossi, M. D. Rossell, N. A. Spaldin, M. Fiebig, and M. Trassin, “Bilateral interface control of nanoscale ferroelectricity,” in preparation (2020).
- ³⁹D. Halwidl, B. Stöger, W. Mayr-Schmölzer, J. Pavelec, D. Fobes, J. Peng, Z. Mao, G. S. Parkinson, M. Schmid, F. Mittendorfer, J. Redinger, and U. Diebold, “Adsorption of water at the SrO surface of ruthenates,” *Nature Mat.* **15**, 450–455 (2016).
- ⁴⁰A. V. Bandura, R. A. Evarestov, and D. D. Kuruch, “Hybrid HF-DFT modeling of monolayer water adsorption on (001) surface of cubic BaHfO_3 and BaZrO_3 crystals,” *Surf. Sci.* **604**, 1591–1597 (2010).

- ⁴¹H. Guhl, W. Miller, and K. Reuter, “Water adsorption and dissociation on SrTiO₃(001) revisited: A density functional theory study,” *Phys. Rev. B* **81**, 155455 (2010).
- ⁴²R. A. Evarestov, A. V. Bandura, and V. E. Alexandrov, “Adsorption of water on (001) surface of SrTiO₃ and SrZrO₃ cubic perovskites: Hybrid HF-DFT LCAO calculations,” *Surf. Sci.* **601**, 1844–1856 (2007).
- ⁴³X. L. Hu, J. Carrasco, J. Klimeš, and A. Michaelides, “Trends in water monomer adsorption and dissociation on flat insulating surfaces,” *Phys. Chem. Chem. Phys.* **13**, 12447–12453 (2011).
- ⁴⁴L. Chen, Z. Cheng, W. Xu, X. Meng, G. Yuan, J. Liu, and Z. Liu, “Electrical and mechanical switching of ferroelectric polarization in the 70 nm BiFeO₃ film,” *Sci. Rep.* **6**, 19092 (2016).
- ⁴⁵C. Gattinoni, I. Efe, and N. Spaldin, “The half polarization quantum in BiFeO₃ and its consequences for thin films and heterostructures,” in preparation (2020).

Supplementary information

Ipek Efe,¹ Nicola A. Spaldin,¹ and Chiara Gattinoni^{1, a)}

*Materials Theory, Department of Materials, ETH Zürich, Wolfgang-Pauli-Strasse 27,
8093, Zürich, Switzerland*

(Dated: 18 March 2024)

arXiv:2010.14895v1 [cond-mat.mtrl-sci] 28 Oct 2020

^{a)}Electronic mail: chiara.gattinoni@mat.ethz.ch

I. CONVERGENCE TEST FOR SLAB THICKNESS

Calculations with the most favorable adsorption sites are carried out for the slab thicknesses of 2–6 unit cells (u.c.) for a water molecule on the charge-compensated slab of Fig. 1b. All atoms were allowed to relax. On the BiO surface the adsorption energy is converged for 4 u.c. On the FeO₂ surface, the absolute values of the adsorption energies are still varying for a slab thickness of 6 u.c., however relative energies between the intact and dissociated structure are already converged at 4 u.c.

Adsorption Energies (eV)				
	FeO ₂ Surface		BiO Surface	
Thickness	Intact	Dissociated	Intact	Dissociated
2 u.c.	-0.788	-0.424	-0.664	-0.617
3 u.c.	-0.593	-0.560	-0.456	-0.425
4 u.c.	-0.804	-0.451	-0.672	-0.642
5 u.c.	-0.787	-0.407	-0.654	-0.624
6 u.c.	-0.784	-0.428		-0.607

TABLE I. Adsorption energy of a water molecule on the compensated surfaces of Fig. 1b with slabs of varying thickness.

II. WATER ON “UNHAPPY” SLAB

Structure of a single water molecule adsorbed on an “unhappy” frozen substrate, Fig. 1.

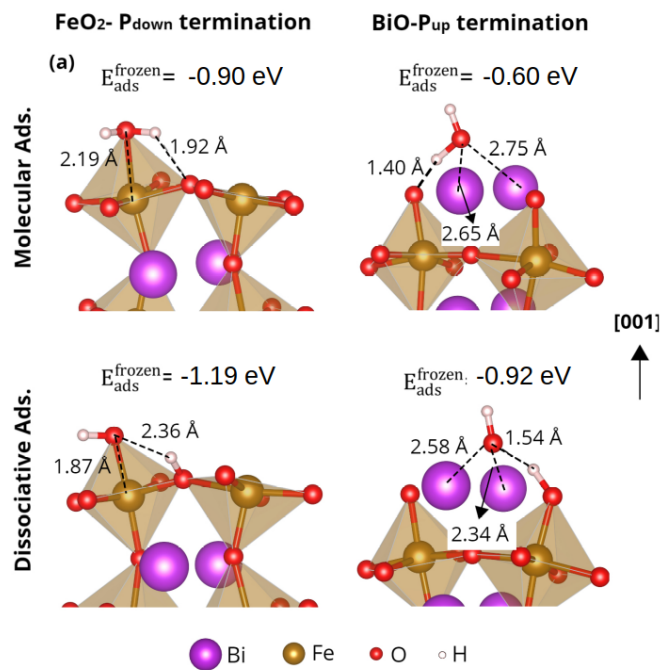


FIG. 1. Most favorable adsorption geometries and the corresponding adsorption energies for a water molecule on the surfaces of frozen unhappy slab.

III. COMPARISON OF WATER ADSORPTION BEHAVIOR ON PEROVSKITES

Reference	Material	Lattice constant (Å)	H ₂ O on AO	H ₂ O on BO ₂	Charged layers	DFT Functional
happy system	BiFeO ₃	3.95	Molecular	Molecular	Yes	optB86b-vdW
unhappy system	BiFeO ₃	3.95	Dissociated	Dissociated	Yes	optB86b-vdW
1	SrTiO ₃	3.94	Dissociated	Dissociated/ Molecular	No	GGA-PBE
2	Sr ₂ RuO ₄	3.9	Dissociated	N/A	No	opt86-vdW
3	SrTiO ₃	3.94	Equal preference	Molecular	No	B3LYP XC
3	SrZrO ₃	4.19	Dissociated	Molecular	No	B3LYP XC
4	BaHfO ₃ BaZrO ₃	4.19	Dissociated	Dissociated	No	PBE0-XC

TABLE II. Comparison of the adsorption modes on different systems and their properties in the literature and this work

REFERENCES

- ¹H. Guhl, W. Miller, and K. Reuter, “Water adsorption and dissociation on SrTiO₃(001) revisited: A density functional theory study,” *Phys. Rev. B* **81**, 155455 (2010).
- ²D. Halwidl, B. Stöger, W. Mayr-Schmölzer, J. Pavelec, D. Fobes, J. Peng, Z. Mao, G. S. Parkinson, M. Schmid, F. Mittendorfer, J. Redinger, and U. Diebold, “Adsorption of water at the SrO surface of ruthenates,” *Nature Mat.* **15**, 450–455 (2016).
- ³R. A. Evarestov, A. V. Bandura, and V. E. Alexandrov, “Adsorption of water on (001) surface of SrTiO₃ and SrZrO₃ cubic perovskites: Hybrid HF-DFT LCAO calculations,” *Surf. Sci.* **601**, 1844–1856 (2007).

Supplementary information

⁴A. V. Bandura, R. A. Evarestov, and D. D. Kuruch, “Hybrid HF-DFT modeling of monolayer water adsorption on (001) surface of cubic BaHfO₃ and BaZrO₃ crystals,” *Surf. Sci.* **604**, 1591–1597 (2010).